Space Weather

RESEARCH ARTICLE
10.1029/2018SW001911

A Study of Intense Local dB/dt Variations During Two Geomagnetic Storms

Chigomezyo M. Ngwira[1,2], David Sibeck[2], Marcos V. D. Silveira[2,3], Marina Georgiou[4,5], James M. Weygand[6], Yukitoshi Nishimura[7,8], and Donald Hampton[9]

[1]Department of Physics, Catholic University of America, Washington, DC, USA, [2]Space Weather Laboratory, NASA Goddard Space Flight Center, Greenbelt, MD, USA, [3]Universities Space Research Association, Columbia, MD, USA, [4]Department of Physics, National and Kapodistrian University of Athens, Athens, Greece, [5]Now at Department of Space and Climate Physics, University College London, Dorking, UK, [6]Institute of Geophysics and Planetary Physics, University of California, Los Angeles, CA, USA, [7]Department of Electrical and Computer Engineering and Center for Space Physics, Boston University, Boston, MA, USA, [8]Department of Atmospheric and Oceanic Sciences, University of California, Los Angeles, CA, USA, [9]Geophysical Institute, University of Alaska, Fairbanks, AK, USA

Abstract Interactions between the solar wind and the Earth's magnetosphere manifest many important space weather phenomena. In this paper, magnetosphere-ionosphere drivers of intense dB/dt produced during geomagnetic storms that occurred on 9 March 2012 and 17 March 2015 are analyzed. A multi-instrument approach combining Time History of Events and Macroscale Interactions during Substorms (THEMIS) mission space-borne and ground-based observations was adopted to examine the magnetosphere-ionosphere signatures associated with the dB/dt extremes during each storm. To complement the THEMIS measurements, ground-based magnetometer recordings and All-Sky Imager observations, equivalent ionospheric currents derived from magnetometer chains across North America and Greenland, and geosynchronous observations from the Los Alamos National Laboratory Synchronous Orbit Particle Analyzer are also examined. Our results show that the most extreme dB/dt variations are associated with marked perturbations in the THEMIS magnetospheric measurements, poleward expanding discrete aurora passing over the magnetometer sites (seen by the ground-based THEMIS All-Sky Imagers), intense Pc5 waves, rapid injection of energetic particles, and intense auroral westward currents. Substorms are considered as the major driver with a possible contribution from magnetospheric waves. The findings of this study strongly suggest that the localization of extreme dB/dt variations is most likely related to the mapping of magnetosphere currents to local ionospheric structures.

Key Points:
- Magnetosphere-ionosphere processes associated with local dB/dt extremes during storms are examined
- Intense dB/dt are confined to poleward edge of expanding aurora, a region with most active but localized magnetosphere energy conversion
- Substorms are considered as the major driver with a possible contribution from magnetospheric waves

Supporting Information:
- Supporting Information S1
- Movie S1
- Movie S2
- Movie S3
- Figure S1
- Figure S2
- Figure S3
- Figure S4
- Figure S5
- Figure S6

Correspondence to:
C. M. Ngwira,
chigomezyo.ngwira@nasa.gov

Citation:
Ngwira C. M., Sibeck, D., Silveira, M. D. V., Georgiou, M., Weygand, J. M., Nishimura, Y., & Hampton, D. (2018). A study of intense local dB/dt variations during two geomagnetic storms. *Space Weather*, *16*, 676–693. https://doi.org/10.1029/2018SW001911

Received 19 APR 2018
Accepted 21 MAY 2018
Accepted article online 24 MAY 2018
Published online 15 JUN 2018

1. Introduction

Space weather-driven geomagnetically induced currents (GICs) flowing in ground-based systems such as high-voltage power transmission networks, oil and gas pipelines, and communication systems are a major concern. The potential impact of space weather on these critical technological assets has prompted renewed interest to further inform our understanding of extreme events. During geomagnetic disturbances, intense time-varying currents produced in the Earth's magnetosphere-ionosphere (M-I) coupled system result in rapid fluctuation of the surface geomagnetic field (dB/dt). A horizontal surface geoelectric field (E field) is induced in the Earth (a conducting medium) fundamentally based on Faraday's law of induction: a changing magnetic field produces an electric field that then drives GIC in man-made electrically conducting technological infrastructure (e.g., Boteler et al., 1998; Pirjola, 2002).

Therefore from a physical standpoint, the E field, which is independent of technological infrastructure, is the primary quantity of interest since it is the basic property that dictates the magnitude of GICs. However, because the major interest of this study is the M-I processes that generate intense geomagnetic perturbations, we employ dB/dt as a proxy for the GIC, thus eliminating the need to determine the E field in the absence of specific (or realistic) ground conductivity model(s) for the region of interest. As previous studies have pointed out, appropriate specification of ground models is critical for GIC applications and cannot be overemphasized (see articles by Bedrosian & Love, 2015; Kelbert et al., 2017; Love, 2012; McKay, 2003).

Understanding the spatiotemporal variation of M-I currents requires a grasp of changes in the driving processes that regulate the state of the whole system. Electric currents in the ionosphere are closely linked to the magnetosphere through large-scale field-aligned currents (FACs). FACs play a key role in the transfer, conversion, and circulation of momentum, mass, and energy between the solar wind, the magnetosphere, and the ionosphere. Enriching our knowledge of the development of dynamic M-I currents during major geomagnetic storms is one of the top priorities in the space weather community today. For GIC studies, it is critical that we understand the complex processes, both external and internal, that regulate currents in the near-Earth space environment (e.g., Adebesin et al., 2016; Ngwira et al., 2015, and references therein).

Several studies show that during geomagnetic disturbances, storm-enhanced high-latitude peak geomagnetic perturbations that cause large GICs tend to be localized (e.g., Boteler & Jansen van Beek, 1999; Pulkkinen et al., 2003, 2015; Ngwira et al., 2015, and references therein). The geomagnetic structures associated with localized extremes at single sites can be greatly different from structures associated with globally or regionally averaged fields (Ngwira et al., 2015; Pulkkinen et al., 2015). Extreme dB/dt variations can significantly impact GICs locally, but the impact on power system stability as a whole is not well understood. In addition, the detailed physical processes that generate these local extremes are not well known.

This paper combines THEMIS (Time History of Events and Macroscale Interactions during Substorms) mission in situ and ground-based observations in a novel way to investigate M-I drivers of two dB/dt extreme events in the Alaskan sector. Additionally, a variety of ground-based observations, ionospheric currents derived from magnetometer chains across North America and Greenland, and geosynchronous observations from the Los Alamos National Laboratory (LANL) Synchronous Orbit Particle Analyzer (SOPA) are also examined to further elucidate the physical processes associated with the extremes. This study emphasizes the need for coordinated multipoint observations to advance our understanding of the extreme dB/dt localization characteristics and space weather in general.

2. Data and Analysis

The primary space-borne and ground-based data sets for the present paper are drawn from several different sources. Because this study is focused on the Alaskan region, we employ NASA's THEMIS mission observations as one of our key sources due to the wide coverage of the region. The THEMIS mission is intended to investigate magnetospheric substorms, which are the manifestation of basic instabilities in the magnetosphere that release energy explosively and drive intense surface E fields. THEMIS combines ground-based and magnetically conjugate in situ observations to determine the generation and large-scale evolution of substorms (e.g., Angelopoulos, 2008; Sibeck & Angelopoulos, 2008). The original mission employed five identical THEMIS satellites that lined up along the Earth's magnetotail to track the motion of particles, plasma, and waves from one point to another and for the first time resolve space-time ambiguities in major regions of the magnetosphere on a global scale.

The North American high-latitude region is well populated with ground-based instrumentation, which we extensively use to characterize the selected events. The THEMIS mission operates two arrays consisting of over 30 magnetometers and 20 All-Sky Imagers (ASIs) around North America, from Alaska to Labrador (Donovan et al., 2006; Mende et al., 2008; Russell et al., 2008). The stations were developed and deployed for a broad coverage of the nightside magnetosphere. A distribution map of THEMIS ground observation sites can be viewed at http://themis.ssl.berkeley.edu/asi_map.shtml. For this case study, 0.5- and 1-s THEMIS geomagnetic field observations were used to compute dB/dt. In addition to the THEMIS data, we also use 60-s INTERMAGNET observations to broaden the ground coverage. We employ dB/dt as a proxy for the induced surface E field in the absence of an appropriate regional conductivity model to realistically determine the E fields.

The spatiotemporal profile of ULF (ultralow-frequency) Pc5 wave activity during the two selected time intervals was examined based on geomagnetic field measurements from a variety of ground-based magnetometer arrays. These include time series of vector magnetic field measurements from the THEMIS ground-based magnetometers (Mende et al., 2008; Russell et al., 2008) and stations from the magnetometer arrays providing data to the SuperMAG collaboration (Gjerloev, 2015). The geomagnetic field measurements from SuperMAG magnetic stations have a temporal resolution of 1 min. A continuous wavelet transform with the Morlet wavelet as the basis function has been applied to analyze the magnetic north component in the time-frequency domain. Prior to the time-frequency analysis using wavelet transforms, a sixth-order high-pass Butterworth filter with a cutoff frequency of 0.9 mHz was applied to obtain the wavelet power spectra covering the Pc5 frequency

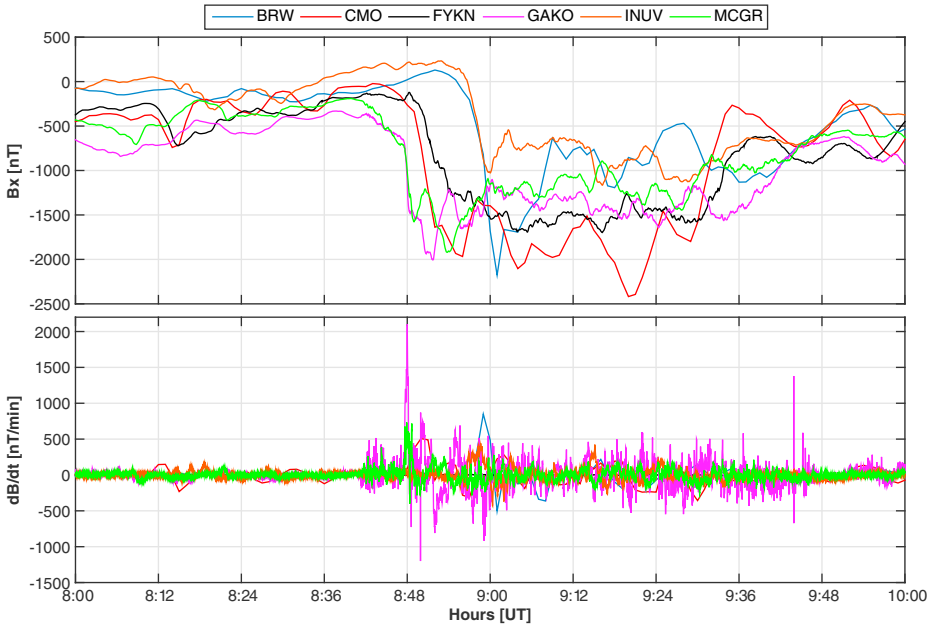

Figure 1. Plot of the geomagnetic B_x component and the rate of change dB/dt at ground sites in the Alaskan sector during the 9 March 2012 storm event. Strong dB/dt consistent with large B_x excursions that are of interest to this study are noted between 08:45 UT and 09:10 UT.

range. Two-dimensional *snapshots* of the weighted sum of wave power contained between 2 and 7 mHz were then derived from all available geomagnetic measurements by interpolation on a rectangular grid of L-shell versus magnetic local time.

LANL geosynchronous electron flux data from the SOPA instrument (Belian et al., 1992; Reeves et al., 1997) are also employed in this study. LANL space environment monitors record the entire 3-D electron distribution from 50 keV to more than 1.5 MeV in one spin. The 10-s time resolution data used in this paper are the local in situ measurements at each satellite (Reeves et al., 2003). To produce the 10-s samples, spin-averaged data were averaged over all three telescopes and then averaged over all spin sectors. This provides a full-sphere measurement but not a true *omnidirectional* measurement. The difference between spin-averaged and omnidirectional measurements is that omnidirectional takes account of both oversampling and undersampling of the 4-pi steradians.

3. Observations and Results

Figure 1 exhibits geomagnetic perturbations observed on the ground for the storm on 9 March 2012. The top panel shows the detrended geomagnetic field B_x component for selected stations in the Alaskan sector at four THEMIS ground recording sites, namely, Fort Yukon (FYKN), Gakona (GAKO), Inuvik (INUV), and McGrath (MCGR). The figure also contains data from two INTERMAGNET network of observatories sites at Barrow (BRW) and College (CMO). The corresponding horizontal $dB/dt = \sqrt{(dB_x/dt)^2 + (dB_y/dt)^2}$ are arrayed in the bottom panel. There are clear spatiotemporal complex patterns seen in this figure with major storm time dB/dt perturbations appearing between 08:45 UT and 09:10 UT (22:45 to 23:10 LT). The largest dB/dt (2100 nT/min) for entire storm period occurs in southern Alaska at GAKO (22:48 LT), and another slightly lower dB/dt enhancement (849 nT/min) is seen about 12 min later at BRW (23:00 LT) in northern Alaska. The dB/dt spatial variations can be caused by nonuniform geomagnetic fields, while the temporal variations are related to time-varying source currents in the M-I system that regulate geomagnetic field fluctuations.

The second event we examine herein occurred during the Saint Patrick's day storm of 17 March 2015. This is the largest storm, as measured by *Dst* index, in the current solar cycle at the time of writing this paper. The rate of change dB/dt calculated for the BRW, CMO, FYKN, and MCGR stations are displayed in Figure 2. Stations FYKN and MCGR were the only two THEMIS ground sites in the Alaskan region of interest that produced the largest dB/dt on this day. However, the highest value of 852 nT/min for the entire storm was experienced at BRW around 03:33 LT. For this storm we are interested in the time period between 13:15 UT and 13:45 UT or

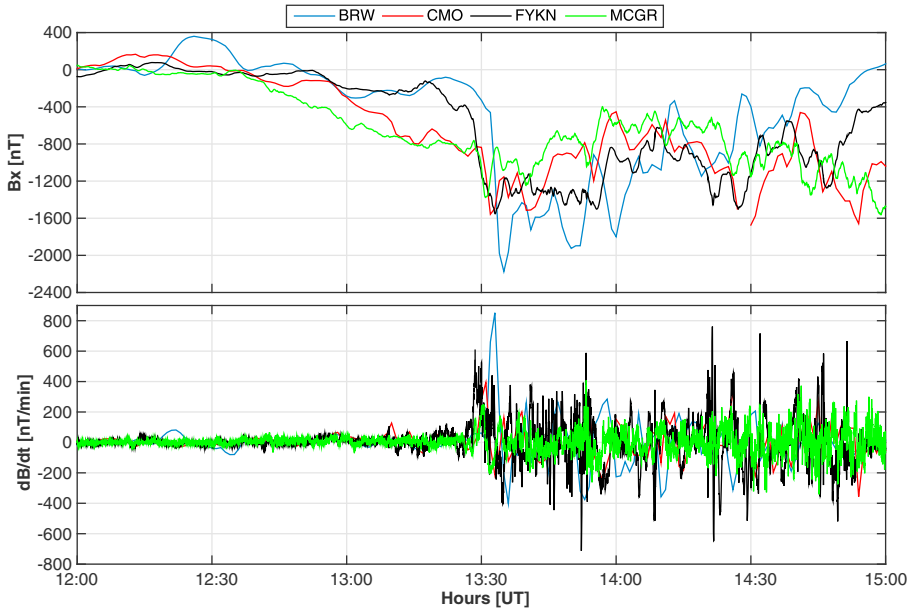

Figure 2. Similar to Figure 1 but only for the sites at BRW, CMO, FYKN, and MCGR during the St. Patrick storm on 17 March 2015. The period of interest is between 13:15 UT and 13:45 UT. BRW = Barrow; CMO = College; FYKN = Fort Yukon; MCGR = McGrath.

0315 LT and 03:45 LT, respectively. In this specific case, the response characteristics are similar to those shown in Figure 1: namely, the timing of steep geomagnetic field excursions coincide with large dB/dt variations.

To understand the dynamics of M-I currents that produce extreme surface dB/dt requires also a knowledge of the external driver processes that regulate the state of the M-I coupled system, which in this case is the solar wind. Figure 3 shows selected interplanetary magnetic field (IMF) and solar wind parameters and the geomagnetic *AE* index. All data are sampled at 1-min time resolution for the two events. The panels show from top to bottom the IMF B_y and B_z components, solar wind bulk speed and number density, and the high-latitude geomagnetic *AE* index. The OMNI definitive IMF and plasma data (GSM) have been time-shifted to the nose of the Earth's bow shock. Panels on the left column of the figure display data from the storm event on 9 March 2012, while the panels in the right column are for the 17 March 2015 storm. The red vertical dashed lines correspond to the onset of sudden *AE* enhancement and large local dB/dt features for each case. It is noted that there was an abrupt increase in the density (>10 particles/cm^3) just prior to the enhancement on 17 March but barely any change on 9 March. However, both cases were associated with strong southward B_z (~ -10 nT), and highly enhanced *AE* values at the same time as the dB/dt amplifications. We note also that the sudden *AE* enhancements are preceded by sharp reversal of the IMF B_y, which was positive in both cases, and marked change of B_z from −5 nT to −20 nT for the 17 March case.

Turning attention to space-based magnetosphere measurements, Figure 4 presents THEMIS D and E observations for the 9 March 2012 storm. From top to bottom the panels show the magnetic field, plasma density and velocity, ion and electron plasma temperatures, SST (solid state telescope) and ESA (electrostatic analyzer) electron flux spectrogram, and electric field. On 9 March THEMIS D and E were both located in the predawn sector of the magnetosphere with ionospheric footprints that mapped down to parts of northeast Canada. The time period shown roughly corresponds to premidnight local times (~22:30 LT) in the Alaskan Yukon sector where the ground events were observed. Between 08:00 UT and 08:30 UT (not shown) the two THEMIS probes detected marked variations in magnetic field, density, velocity, and electric field that were increased, while temperature and electron flux decreased, but the corresponding surface dB/dt do not show significant changes. However, between 08:45 UT and 09:10 UT both THEMIS probes again encountered increased levels of fluctuation. At about 08:46 UT, an increase in the magnetic field B_y and B_z was detected by both probes, and approximately 3 min later dB/dt reveal major changes at the four ground sites. The largest perturbations are seen close to 08:58 UT (22:58 LT in Alaska) preceding the peak dB/dt at BRW around 23:00 LT (09:00 UT). The goal of this study is to gain insight on the physical processes associated with these extreme dB/dt variations.

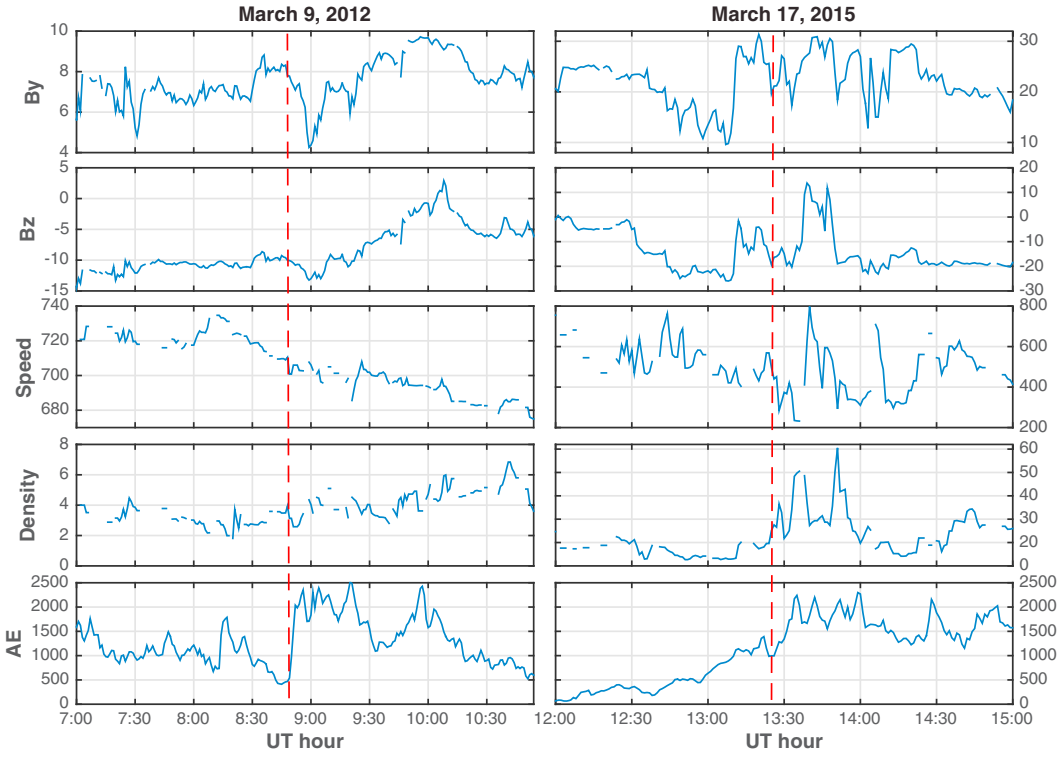

Figure 3. OMNI interplanetary solar wind data and auroral electrojet index. (from top to bottom) IMF B_y, IMF B_z, bulk speed, number density, and the *AE* index. (left column) On 9 March 2012 and (right column) 17 March 2015. The vertical red dashed lines indicate the onset of sudden *AE* enhancement for each storm event. IMF = interplanetary magnetic field.

Figure 5 displays THEMIS observations for the event on 17 March 2015. For this event, the interval of interest is between 13:00 UT and 1400 UT during which THEMIS probes D and E detected magnetic field, density, velocity, temperature, flux, and electric field variations. During this time interval both THEMIS D and E were located on the dusk side with footprints over northern Russia. At the same time, corresponding dB/dt at FYKN and MCGR show a marked response around postmidnight local times (~03:30 LT or 13:30 UT). We note that the two probes D ($X = 2.5$, $Y = 7.5$, and $Z = -2.0$, GSE) and E ($X = 0.1$, $Y = 5.2$, and $Z = -1.5$, GSE) appear to observe major magnetic field variations at slightly different times with probe D, having the largest variations ($\Delta > 100$ nT), detecting strong perturbations starting just before 13:30 UT. Probe D observed plasma flowing tailward (negative velocity in x direction) with a velocity reaching about 400 km/s at 13:30 UT. This could be related to a compression of the dayside magnetosphere by a strong pressure pulse as indicated in solar wind data. On the other hand, probe E detected slightly smaller magnetic field perturbations ($\Delta < 50$ nT) shortly after 13:30 UT. In this case, the perturbations are associated with fast sunward flows (positive velocity in x direction) with velocity around 80 km/s at 13:40 UT. Another evident difference is that the high-intensity THEMIS electric field wave measurements for probe D are seen over an extended interval (~ 13:10–13:45 UT) while the probe E measurements are only confined to a narrow time instance approximately centered around 13:40 UT.

In Figure 6 we present a comparison between dB/dt and the THEMIS ASI auroral keogram for 9 March 2012. The figure shows the substorm timing and poleward expansion more easily. The timing of substorm poleward expanding aurora passing over the magnetometer stations matches very well with dB/dt peaks. The aurora was intense first and then weakened as it propagated poleward, consistent with the largest dB/dt near the substorm onset location. Comparison of dB/dt and the Toolik ASI auroral keogram during the storm event on 17 March 2015 are shown in Figure 7. Toolik is located midway between FYKN and BRW. Auroral brightening and poleward expansion are clearly seen. The 13:29 UT intense dB/dt at FYKN nicely corresponds to a weak

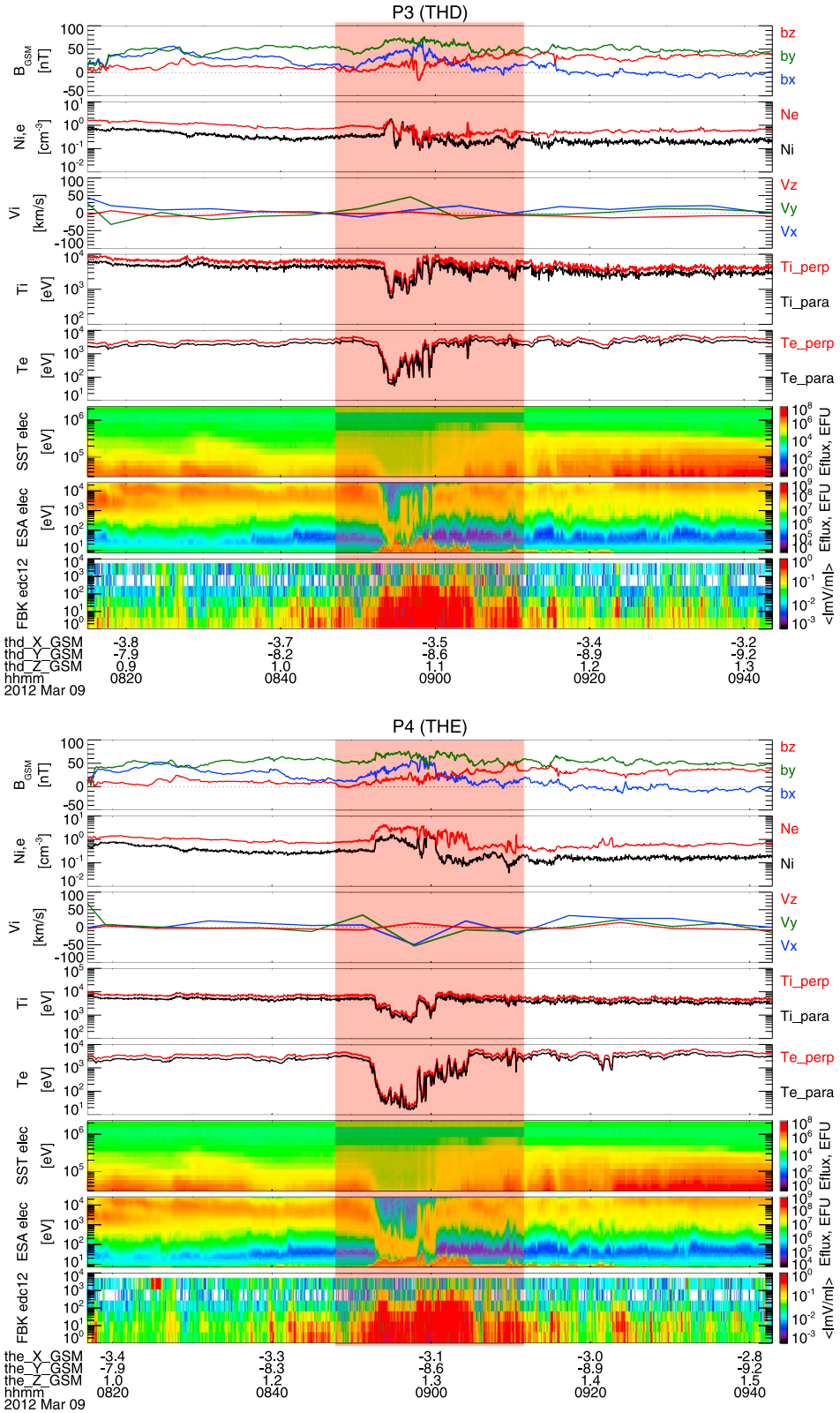

Figure 4. Observations by THEMIS spacecraft lying on the postmidnight magnetosphere during the event on 9 March 2012. The top exhibit contains THEMIS-D observations, while the bottom exhibit contains THEMIS-E probe data. The interval of interest (shaded area) is between 08:30 and 09:30 UT. THEMIS = Time History of Events and Macroscale Interactions during Substorms.

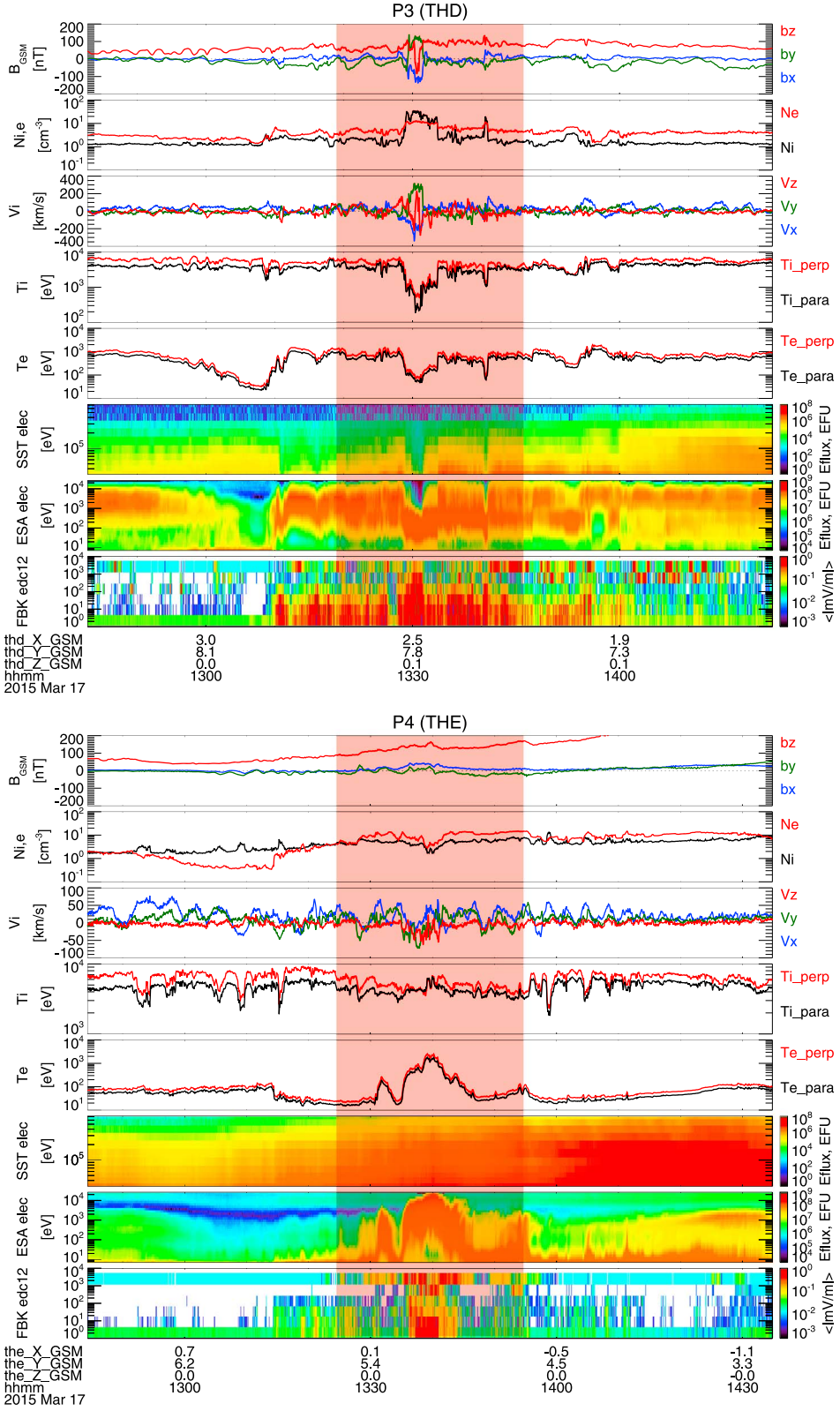

Figure 5. Observations of THEMIS spacecraft as in Figure 4 but for 17 March 2015. In this case, the two THEMIS probes where located in the post noonside magnetosphere. The interval of interest is between 13:00 and 14:00 UT. THEMIS = Time History of Events and Macroscale Interactions during Substorms.

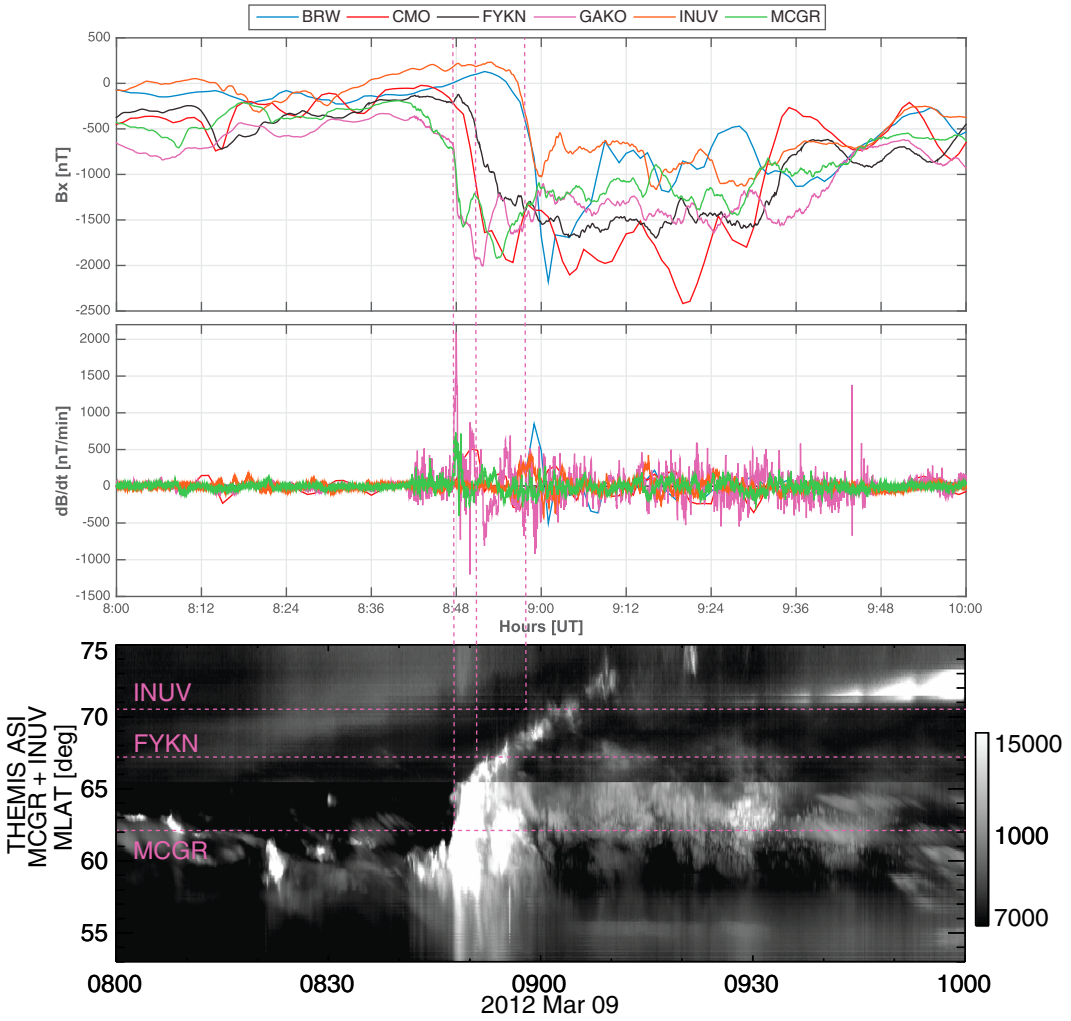

Figure 6. Comparison of dB/dt and auroral keogram for the event on 9 March 2012. The THEMIS ASI observations from MCGR and INUV are displayed. The plot clearly shows that the dB/dt peaks are consistent with the substorm timing and poleward expansion. THEMIS ASI = Time History of Events and Macroscale Interactions during Substorms All-Sky Imager; MCGR = McGrath; INUV = Inuvik.

auroral brightening localized to the FYKN latitude, and then the 13:32 UT large dB/dt at BRW matches with the intense auroral brightening and poleward expansion. Based on these data, the story of this second event is consistent with the first event. Additionally, dB/dt movies and the THEMIS ASI mosaic movie (9 March) are provided in the supporting information and discussed in the following section.

We now examine the response of auroral ionospheric currents over North America with the aid of equivalent ionospheric current (EIC) maps derived using the state-of-the-art spherical elementary current systems (SECS) technique developed by Amm and Viljanen (1999). The SECS technique is based on a singular value decomposition method by which recorded ground magnetic field fluctuations are inverted to determine the ionospheric current system. Weygand et al. (2011) first adapted this approach for large nonrectangular regions with widely separated ground magnetometers (~350 km) by applying it to the whole North American auroral region. The EIC maps provided here have a resolution of ~3° (about 175 km) in GLAT (geographic latitude) and ~7° in GLON (geographic longitude). The maps inferred at the time resolution of the database, in this case 10 s, show in detail the dynamic evolution of the currents over the entire North American ground magnetometer network and can therefore be analyzed further in conjunction with near-simultaneous images of the THEMIS ASI mosaics and/or keograms (Weygand et al., 2011).

Figures 8a and 8c show EIC maps for North America and Greenland for the activity on 9 March 2012. The vector fields show the strength of ionospheric currents for specific ground magnetometer sites at 08:47 UT and 08:49

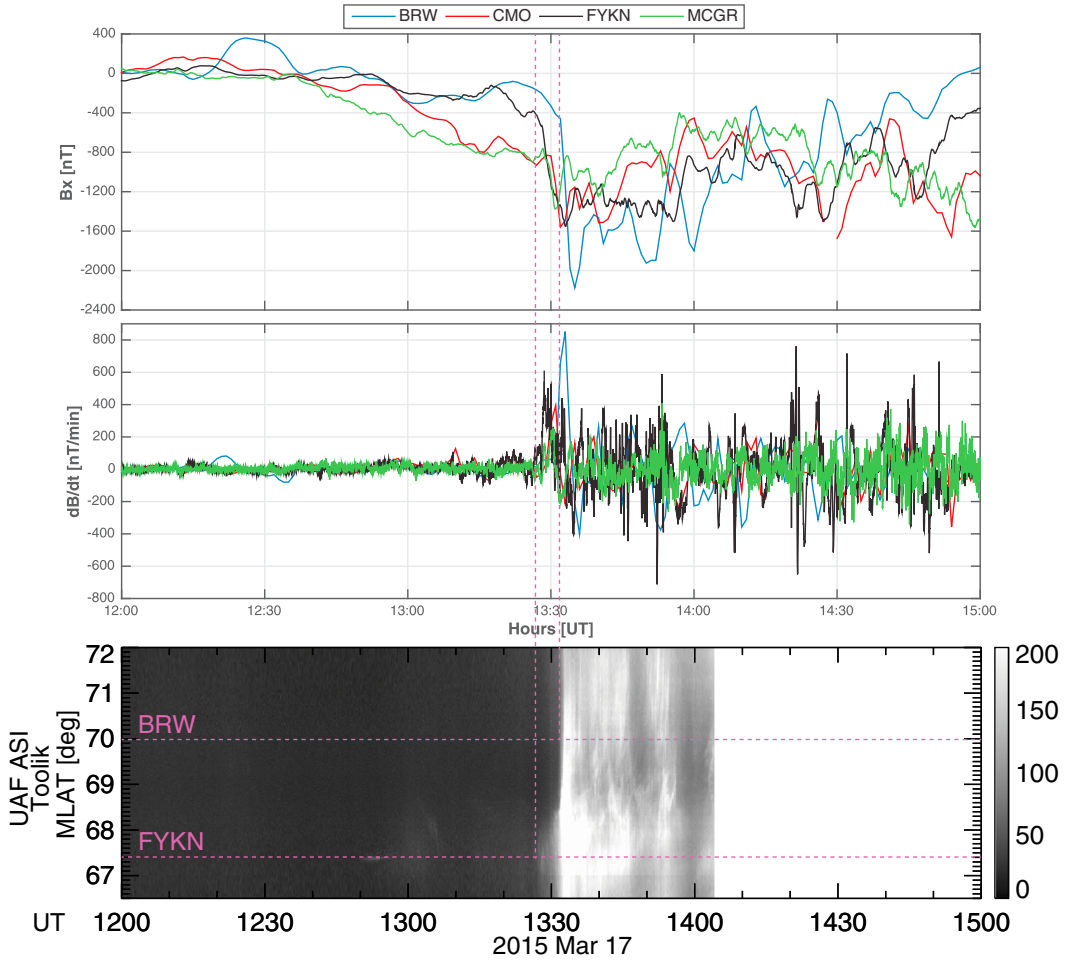

Figure 7. Same as Figure 6 but for the event on 17 March 2015. The ASI observations from Toolik, located midway between FYKN and BRW, are shown. Note that there is no ASI data after 14:05 UT. ASI = All-Sky Imager; FYKN = Fort Yukon; BRW = Barrow.

UT, respectively. At 0847 UT a moderate (750 mA/m) westward current prevails over the Alaskan sector. But later on at 08:49 UT much stronger (1,900 mA/m) westward currents develop following a substorm onset just before 08:47 UT as seen from the THEMIS ASI keogram in Figure 6. Strong westward current extends from the Hudson Bay area to Alaska, but the strongest currents are located over Alaska. North of this current system is a moderate (300 mA/m) eastward current. Figures 8b and 8d display large-scale FACs, where the blue plus symbols indicate upward current amplitudes and the red squares indicate the downward current amplitudes. Figure 9 generally shows similar response characteristics as in Figure 8; however, we note that the westward current system extends over a wider area of Alaska. This could be related to the strength of the magnetic storms since the 17 March storm was larger in scale than the 9 March storm. Interestingly for both storms, the ground footprint of the EICs appear to be at the interface/boundary of the upward currents in the southern half and downward currents in the northern half. This emphasizes the role of the ionosphere in the coupling of the solar wind-magnetopshere-ionosphere system by connecting the upward and downward FACs.

In Figure 10, we present geosynchronous SOPA energetic electron measurements for the LANL-01A satellite during the event on 17 March 2015. The spacecraft was at postmidnight local times having crossed local midnight at about 11:30 UT. Three different energy channels, E5, E6, and E7, respectively representing the values 275, 395, and 577 keV, are plotted. One can clearly see (Figure 10) two large enhancements of electron flux (injections), as indicated by the two vertical dashed lines at ~13:25 UT and ~13:32 UT, which are preceded by a growth phase flux *dropout* from about 13:08 UT to 13:24 UT and from 1330 UT to 1332 UT, respectively. The flux growth phase dropout is caused by the tailward stretching of the magnetic field near local midnight (Reeves & Henderson, 2001). It should be noted that the timing of the electron injections described here are in

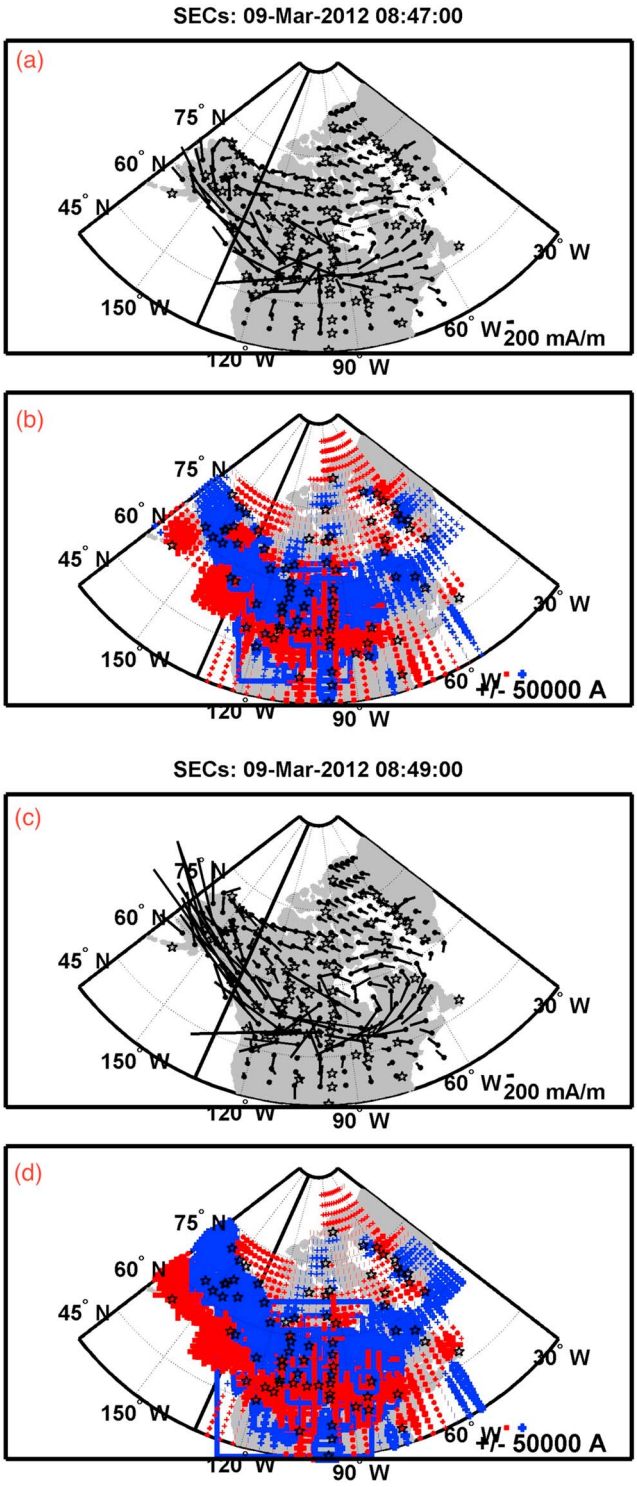

Figure 8. Equivalent ionospheric current maps (a and c) for North America as derived using the SECS method for 9 March 2012. (b and d) The corresponding field-aligned currents (color). Two specific time steps at 08:47 and 08:49 UT are highlighted. The black line indicates the location of local midnight. The stars mark the locations of ground magnetometer stations providing the data for that day. SECS = spherical elementary current systems.

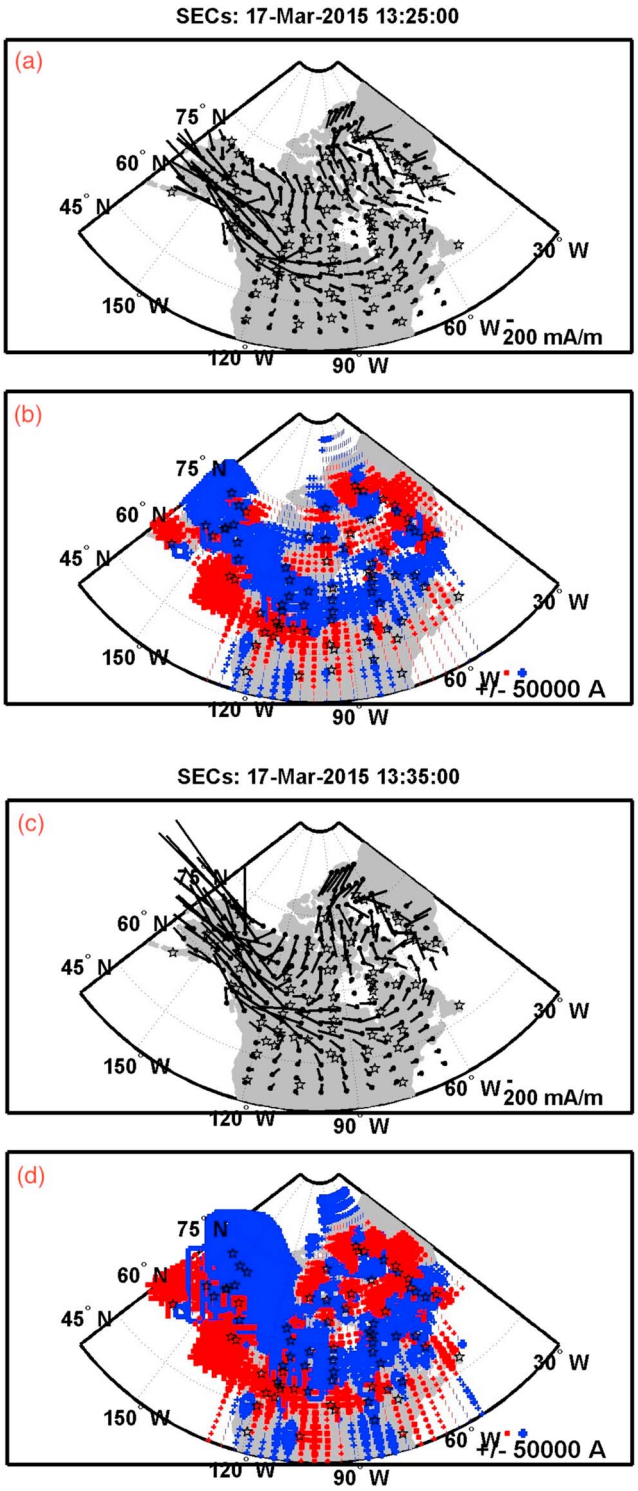

Figure 9. The same format as Figure 8 but for 17 March 2015.

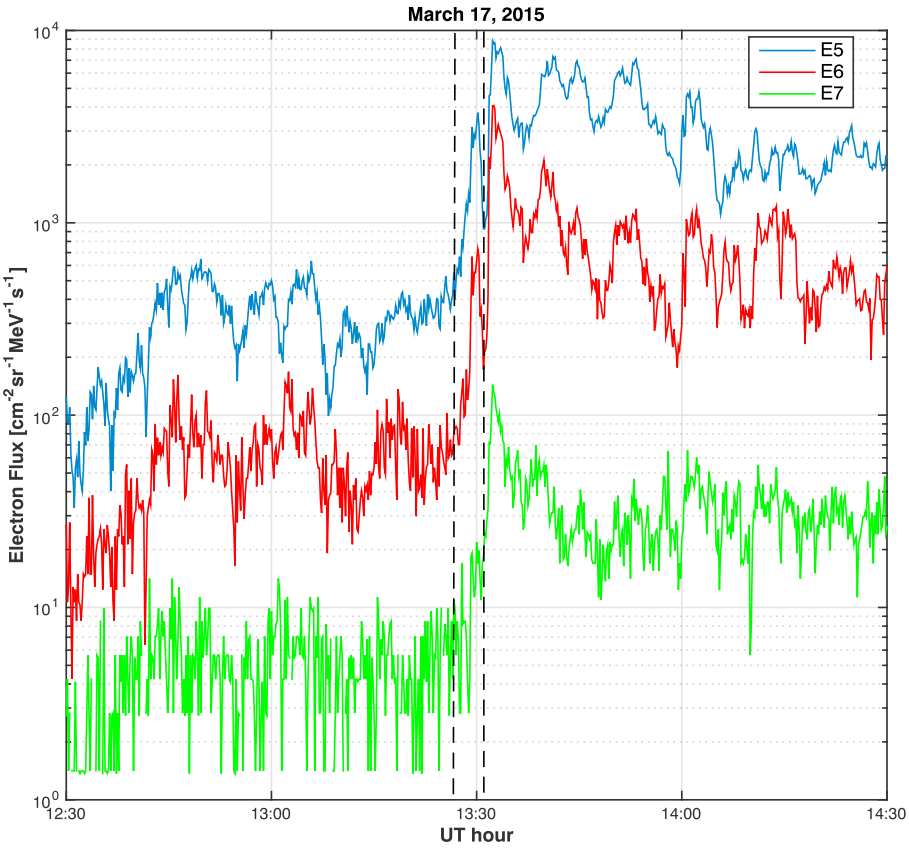

Figure 10. Geosynchronous SOPA energetic electron measurements during the geomagnetic storm on 17 March 2015. The LANL-01A satellite data for three different energy channels E5, E6, and E7, which represent the values 275, 395, and 577 keV, respectively, are plotted. The spacecraft crossed local midnight at about 11:30 UT. The dashed lines indicate the times of extreme surface dB/dt. Data courtesy of Geoffrey Reeves. SOPA = Synchronous Orbit Particle Analyzer; LANL = Los Alamos National Laboratory.

good agreement with THEMIS D and E ESA electron flux observations in Figure 5. On the ground, the particle injections can be closely connected to substorm onset identified by the sharp bays in the B_x component of magnetic field at FYKN, MCGR, CMO, and BRW, as shown in Figure 2. Also, the well-defined double injection is evident in the dB/dt response at FYKN (Figure 2) with peaks at 13:30 UT and 13:35 UT. This is an interesting result because it shows that there is a strong connection between dB/dt amplification and complex internal magnetospheric processes.

We also investigate ULF Pc5 wave activity by applying wavelet transform to measurements from multiple magnetometer arrays covering a wide range of magnetic longitudes and latitudes made available through the worldwide collaboration SuperMAG, as described in section 2. The local time of peaks observed in these Pc5 wave activity profiles over the Alaska sector stations KAV (Kaktovik), BRW, FYU (Fort Yukon), PKR (Poker Flats), CMO, GAK (Gakona), T40 (McGrath), T39 (Trapper Creek), and SHU (Shumagin) (at ~2245 LT on 9 March 2012 and ~03:30 LT on 17 March 2015) are consistent with intense dB/dt. Much of the wave activity is concentrated in the premidnight and postmidnight sectors; this asymmetric distribution around noon has been seen in statistical studies (i.e., Rae et al., 2012).

4. Discussion

This study combines multipoint space-borne and ground-based measurements to study the magnetosphere and ionosphere response characteristics associated with extreme dB/dt events during two geomagnetic storms. These two geomagnetic storms produced the largest high-latitude dB/dt values in the current solar cycle, specifically in the Alaska region. Table 1 provides a summary of noteworthy observations that lays out a series of events leading up to the period of peak dB/dt cases. In this section we discuss the results and what they mean and the direction of future research efforts.

Table 1
Summary of Key Observations Arraying the Progression of Events

UT (hh:mm)	Description of event
9 March 2012	
08:46	Sudden auroral brightening seen from THEMIS ASI
08:47	THEMIS D and E magnetic field B_z starts to increase
08:48	Sudden *AE* and *AL* enhancement
08:48	Large peak dB/dt values over Alaska but extreme value at GAKO
08:49	Appearance of enhanced EICs over Alaska
08:49	Start of Pc5 wave activity enhancement over Alaska
08:58	Large peak dB/dt at BRW
17 March 2015	
13:23	Substorm onset according to SuperMag event list
13:25	THEMIS D and E magnetic field B_z starts to increase
13:25	LANL-01A first injection
13:28	Start of ASI saturation at FYKN
13:28	Start of Pc5 wave activity enhancement
13:30	Strongly enhanced EICs appear in northern Alaska (not shown)
13:30	Large peak dB/dt at FYKN
13:31	Large peak dB/dt at MCGR
13:32	LANL-01A second injection
13:33	Second peak dB/dt at FYKN and a peak at CMO
13:35	Strongly enhanced EICs appear in northern Alaska
13:35	Extreme dB/dt at BRW

Note. THEMIS ASI = Time History of Events and Macroscale Interactions during Substorms All-Sky Imager; LANL = Los Alamos National Laboratory; EIC = equivalent ionospheric current; GAKO = Gakona; BRW = Barrow; FYKN = Fort Yukon; MCGR = McGrath; CMO = College.

Careful examination of the THEMIS (http://themis.ssl.berkeley.edu/summary.php) and IMAGE (International Monitor for Auroral Geomagnetic Effects, http://space.fmi.fi/image/beta/) ground-based magnetometer online magnetograms (see supporting information) shows typical substorm features that existed on both 9 March 2012 and 17 March 2015, particularly during our periods of interest. Both THEMIS and IMAGE ground networks cover the magnetic latitudes where the electrojet currents related to substorms flow. The IMAGE signatures are weak (~300 nT amplitude) for 9 March, with mainly positive (eastward) perturbations, but relatively strong (~700 nT) deviations for 17 March. By contrast, the THEMIS magnetometer data indicate that intense westward electrojet currents (negative perturbations with > 1,000 nT amplitude) were present on both days. It is worth noting that the IMAGE chain is located in early morning and afternoon for 9 and 17 March, respectively, while THEMIS Alaska chain is near local midnight in both cases. Our interpretations of auroral currents are fully supported by EIC maps in Figures 8 and 9 and by the sudden large *AE* (or *AL*, not shown) index jump in both scenarios, as highlighted in Figure 3. Historically, the *AE* index has been interpreted as an indicator of auroral electrojet activity (e.g., Gjerloev et al., 2004). Altogether these features are consistent with substorms, which are one of the major agents in coupling the magnetosphere and the ionosphere (Akasofu, 1981; Borovsky & Funsten, 2003; Ebihara et al., 2005; Nishimura et al., 2010; Wolf, 1975, and references therein).

One can therefore assert that the extreme surface dB/dt cases presented here are caused by auroral electrojet current, a dominant player in the auroral zone induction process. Magnetospheric substorms create the most intense auroral currents and have long been recognized as among the leading geo-effective causes of large-amplitude high-latitude surface E fields (e.g., Ngwira et al., 2014; Pulkkinen et al., 2005; Viljanen et al., 2006, and references therein). Substorms are elementary physical processes of solar wind energy storage and explosive release in Earth's magnetotail region, which encompass fundamental plasma physics questions. The most remarkable auroral substorm feature is the sudden brightening and poleward expansion of the aurora. Closely coupled with this expansion is an intense westward auroral electrojet current across the bulge of expanding aurora (McPherron & Chu, 2016), which is a direct manifestation of the substorm current wedge

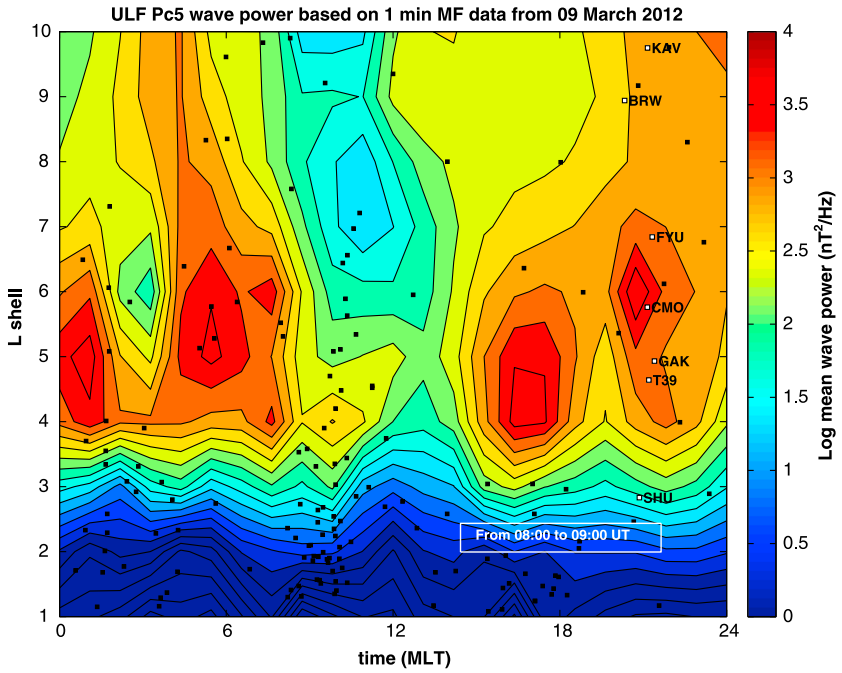

Figure 11. Profile of Pc5 wave activity during the event on 9 March 2012. Plot shows activity as a function of the magnetic local time (MLT) and L-shell values. Locations of ground magnetometer sites are given by black squares, while those in the Alaskan sector used for this study are highlighted in white squares.

(e.g., Murphy et al., 2013; Yao et al., 2012, and references therein). The substorm current wedge is a central element of the substorm expansion phase associated with magnetic field dipolarization in the magnetotail following substorm onset consisting of downward FACs in the east, upward FACs in the west, and an enhanced westward electrojet in the ionosphere (McPherron et al., 1973).

Additional satellite observations of the magnetospheric status are in good agreement with the ionospheric signatures of the substorm (or associated ground dB/dt enhancement). SOPA data from LANL-01A satellite (Figure 10) show an energetic electron flux dropout and rapid two-peak injection whose timing coincides with the surface dB/dt response at FYKN and MCGR magnetometer sites, as seen in Figure 2. The main factors that are considered to cause dropouts are the substorm growth phase and solar wind dynamic pressure. It is important to note that storms are not necessary for presence of dropouts, but dropouts are often seen during substorm activity (e.g., Boynton et al., 2016; Reeves & Henderson, 2001). On the other hand abrupt compression of the magnetosphere due to an increase in dynamic pressure causes trapped electrons in the outer radiation belt to be lost to the solar wind via magnetopause shadowing (e.g., Bortnik et al., 2006; Boynton et al., 2016; Kim & Chan, 1997; Onsager et al., 2004; Reeves et al., 2003, and references therein).

In contrast, the explicit mechanism by which the magnetosphere is able to energize radiation belt electrons has also been particularly challenging to resolve. The conventional theory is that large-scale, fluctuating electric and magnetic fields energize particles through radial diffusion (Chen et al., 2007). THEMIS spacecraft observations show that the timing of rapid magnetic field reconfiguration and particle injections (also LANL-01A) correspond well with dB/dt enhancements. Energetic particle injections (tens to hundreds of keV) are characteristic features of substorm onset and play a key role in the dynamics of the inner magnetosphere (Baker et al., 2016; Chen et al., 2007; Liu et al., 2016), especially during magnetic storms. They are a seed population for the radiation belt and ring current and create particle velocity space anisotropies that drive kinetic waves responsible for particle losses or further acceleration in the inner magnetosphere (Liu et al., 2016). Reconfiguration of tail magnetic fields and substorm injections are highly complex processes, and knowledge of such events is therefore crucial to answering important questions about inner magnetosphere dynamics and production of extreme dB/dt.

Additionally, observations show that during geomagnetic storms magnetospheric wave dynamics are closely linked to those of particles (e.g., Chen et al., 2007; Friedel et al., 2002, and references therein), and various

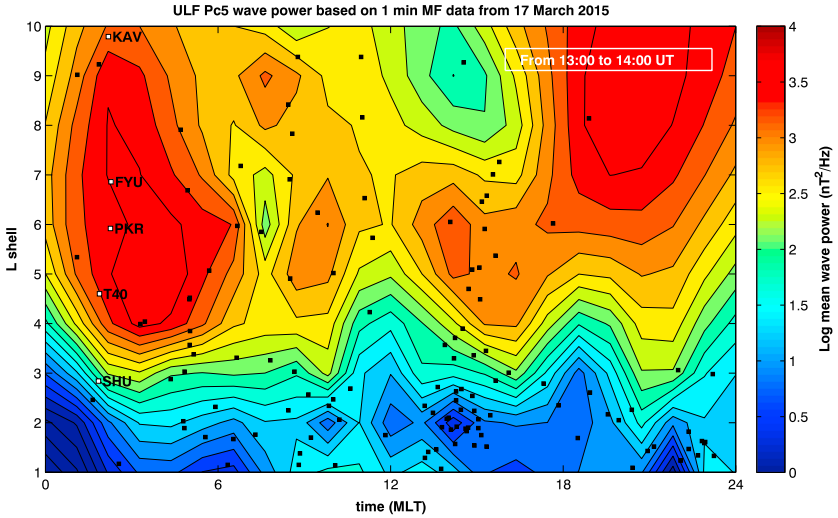

Figure 12. Profile of Pc5 wave activity during the event on 17 March 2015.

kinds of interrelationships can occur. In this study, Figures 11 and 12 demonstrate that intense Pc5 wave activity centered around the ground stations in Alaska was present. Several studies show a strong connection between the geomagnetic pulsations and GIC events (Pulkkinen & Kataoka, 2006; Pulkkinen et al., 2005). In general, the most intense Pc5 waves, with amplitudes about an order of magnitude larger than common Pc5 pulsations, are observed during the recovery phase of severe magnetic storms. These are commonly called global Pc5 pulsations because they can be observed simultaneously in the morning and evening sectors over a wide range of latitudes (e.g., Marin et al., 2014). In addition, these ULF waves have amplitudes as large as the changes that occur in association with auroral zone disturbances, such as substorms. Lyons et al. (2002) argue that large-scale Pc5 waves are a major component of the tail dynamics during periods of enhanced convection. However, what is still not quite clear is the role/contribution of these waves in the generation of extreme dB/dt. As Onsager et al. (2004) point out, one of the challenges that make it difficult to explain the exact causes is that several different mechanisms can be contributing. Therefore, going forward, the key challenge is to isolate and understand the role of each mechanism in driving extreme events.

Another major outstanding question surrounding GICs concerns the localization of the ground response. As we have shown here using widely separated THEMIS spacecraft, the magnetosphere signatures of the two events are global in nature but the ground footprint of the extremes is clearly localized with spatial scales of a few hundred kilometers. This agrees with an earlier report by Ngwira et al. (2015) who provides further evidence (12 storms) for the localized nature of these events. Upon closer inspection of Figures 1 and 2, it is clear that intense dB/dt events on both 9 and 17 March first appear in the southern parts of Alaska at GAKO and MCGR, followed by central locations at CMO and FYKN, then later at the most northern locations BRW and INUV. This characteristic is consistent with the poleward expansion of the auroral currents associated with substorms, which would perhaps suggest that the location of the substorm onset is in the near vicinity of southern Alaska. Figures 6 and 7 show that intense dB/dt are confined to the poleward edge of the poleward-expanding discrete aurora. This corresponds to the region of most powerful aurora during a substorm, a region where energy conversion in the magnetosphere is most active but localized. Wygant et al. (2000) show using space-based evidence that intense electric field and Poynting flux occurs at the poleward edge. Therefore, it is highly likely that extreme dB/dt could be associated with this localized system.

On the ground, THEMIS ASI mosaic movies (see Movie S1 of supporting information) also contain evidence of bright auroral arc features at MCGR between 08:45 and 08:54 UT on 9 March. In this specific case the substorm onset (sudden brightening of aurora) and growth is clearly confined to a subsector of the Alaskan region but poleward expansion of the auroral arc can be seen, as revealed in the supporting information movie. Furthermore, on 17 March saturated THEMIS keogram images (see Figure S6 of supporting information) in combination with EIC maps (Figure 9) confirm that strong auroral westward current was directly overhead at the specific sites. This implies that our ground sites were in the near vicinity to the substorm onset

location (or source region for the localization), which strongly suggests a source current related to the existence of small-scale/isolated ionospheric processes or structures (e.g., Boteler & Jansen van Beek, 1999; Tsurutani et al., 2015). Despite this evidence, it is still not clear if substorms are the primary/seeding mechanism for the localization, but a thorough community-wide effort is encouraged to further explore these processes.

Finally, we draw attention to a recent investigation on *supersubstorms* (extremely intense) by Tsurutani et al. (2015). They show that these extremely intense isolated events appear to be externally triggered by small regions of very high density solar wind plasma cloud striking the magnetosphere. Tsurutani et al. (2015) further hypothesized that southward IMF B_z is a necessary condition for loading energy into the magnetosphere/magnetotail, while the plasma clouds trigger the release of the stored energy. For substorms, only a small fraction typically lead to extreme geomagnetic field fluctuations, therefore, examining the development and evolution of these supersubstorms could prove important for enriching our understanding of the relationship between substorms and extreme GICs, and in our view, these are the kind of events that the GIC community ought to pay much more attention to. However, it is important to note that at the present moment there is no direct evidence linking these supersubstorms to extreme GICs.

5. Summary and Conclusions

Even though our understanding of space weather has significantly grown over the last two decades, one of the major challenges the GIC community continues to encounter is understanding the physical processes that cause local surface dB/dt extremes, which could in turn produce large GICs. The two case studies presented here have allowed us to see the ground geomagnetic response, to observe large-scale magnetosphere dynamics and to characterize the development and evolution of ionospheric currents.

Our results show a strong connection between auroral processes and the development of extreme surface dB/dt, which strongly supports substorm-related activity as the major driving mechanism for the two storms in the present study. However, it is still not clear at present whether substorms are the primary seeding mechanism for strong dB/dt since the effects of substorms are widespread in nature but extreme dB/dt are localized. Our findings strongly suggest that the localization of surface dB/dt is most likely related to the mapping of magnetosphere currents to local ionospheric structures. In addition, we have shown that strong Pc5 activity was present during these events. The role of Pc5 pulsations in driving extreme dB/dt is complicated and unclear; therefore, more investigations need to be performed to distinguish how surface dB/dt response is impacted by this activity.

Lastly, even though there is a clear association between the extreme surface dB/dt and various observations/measurements shown here, more work needs to be done, and we encourage space weather researchers to undertake such efforts. A more comprehensive coordinated ground-based and space-borne investigation is required to create a better picture of the external/internal triggers of localized intense dB/dt events and their relation to substorms and other processes. We recommend placing particular emphasis on the need to understand the spatial and temporal characteristics of localized dB/dt drivers.

Acknowledgments
The authors would like to acknowledge useful discussions with Antti Pulkkinen, Geoffrey Reeves, Hyunju Connor, Kyle Murphy, Stephen Mende, Harald Frey, and Mike Ruohoniemi. THEMIS is funded under NASA contract NAS5-02099. The THEMIS mission team is acknowledged for use of data from the mission. Deployment of the THEMIS ASIs was partly supported by the Canadian Space Agency contract 9F007-046101. The FYKN magnetometer is operated as part of the University of Alaska Geophysical Institute Magnetometer Array. The OMNI data are made available via the NASA Goddard Space Flight Center Space Physics Data Facility (http://cdaweb.gsfc.nasa.gov/). The results presented in this paper rely on data collected at magnetic observatories. We thank the national institutes that support them and INTERMAGNET for promoting high standards of magnetic observatory practice (www.intermagnet.org). The ULF Pc5 analysis was performed using SuperMAG global ground-based magnetometer data. SuperMAG is made possible by the generous funding provided by the NSF and NASA. The data are available at http://supermag.jhuapl.edu/. The effort at the Catholic University of America (CUA) is supported by NASA grant NNG11PL10A 670.157 to CUA/IACS.

References

Adebesin, B. O., Pulkkinen, A., & Ngwira, C. M. (2016). The interplanetary and magnetospheric causes of extreme d*b*/d*t* at equatorial locations. *Geophysical Research Letters*, *43*, 11,501–11,509. https://doi.org/10.1002/2016GL071526

Akasofu, S.-I. (1981). Energy coupling between the solar wind and magnetosphere. *Space Science Reviews*, *28*, 121–190.

Amm, O., & Viljanen, A. (1999). Ionospheric disturbance magnetic field continuation from the ground to the ionosphere using spherical elementary current systems. *Earth Planets and Space*, *51*, 431–440.

Angelopoulos, V. (2008). The THEMIS Mission. *Space Science Reviews*, *141*, 5–34. https://doi.org/10.1007/s11214-008-9336-1

Baker, D. N., Jaynes, A. N., Turner, D. L., Nakamura, R., Schmid, D., Mauk, B. H., et al. (2016). A telescopic and microscopic examination of acceleration in the June 2015 geomagnetic storm: Magnetospheric Multiscale and Van Allen Probes study of substorm particle injection. *Geophysical Research Letters*, *43*, 6051–6059. https://doi.org/10.1002/2016GL069643

Bedrosian, P. A., & Love, J. J. (2015). Mapping geoelectric fields during magnetic storms: Synthetic analysis of empirical United States impedances. *Geophysical Research Letters*, *42*, 10,160–10,170. https://doi.org/10.1002/2015GL066636

Belian, R. D., Gisler, G. R., Cayton, T., & Christensen, R. (1992). High-Z energetic particles at geosynchronous orbit during the great solar proton event series of October 1989. *Journal of Geophysical Research*, *97*(A11), 16,897–16,906.

Borovsky, J. E., & Funsten, H. O. (2003). Role of solar wind turbulence in the coupling of the solar wind to the Earth's magnetosphere. *Journal of Geophysical Research*, *108*(A6), 1246. https://doi.org/10.1029/2002JA009601

Bortnik, J., Thorne, R. M., O'Brien, T. P., Green, J. C., Strangeway, R. J., Shprits, Y. Y., & Baker, D. N. (2006). Observation of two distinct, rapid loss mechanisms during the 20 November 2003 radiation belt dropout event. *Journal of Geophysical Research*, *111*, A12216. https://doi.org/10.1029/2006JA011802

Boteler, D. H., & Jansen van Beek, G. (1999). August 4, 1972 revisited: A new look at the geomagnetic disturbance that caused the L4 cable system outage. *Geophysical Research Letters*, *26*(5), 577–580.

Boteler, D. H., Pirjola, R. J., & Nevanlinna, H. (1998). The effects of geomagnetic disturbances on electrical systems at the Earth's surface. *Advances in Space Research*, *22*(1), 17–27.

Boynton, R. J., Mourenas, D., & Balikhin, M. A. (2016). Electron flux dropouts at geostationary Earth orbit: Occurrences, magnitudes, and main driving factors. *Journal of Geophysical Research: Space Physics*, *121*, 8448–8461. https://doi.org/10.1002/2016JA022916

Chen, Y., Reeves, G. D., & Friedel, R. H. W. (2007). The energization of relativistic electrons in the outer Van Allen radiation belt. *Nature Physics*, *3*, 614–617. https://doi.org/10.1038/nphys655

Donovan, E., Mende, S., Jackel, B., Frey, H., Syrjaäsuo, M., Voronkov, I., et al. (2006). The THEMIS all-sky imaging array—System design and initial results from the prototype imager. *Journal of Atmospheric and Solar-Terrestrial Physics*, *68*, 1472–1487.

Ebihara, Y., Fok, M.-C., Sazykin, S., Thomsen, M. F., Hairston, M. R., Evans, D. S., et al. (2005). Ring current and the magnetosphere-ionosphere coupling during the superstorm of 20 November 2003. *Journal of Geophysical Research*, *110*, A09S22. https://doi.org/10.1029/2004JA010924

Friedel, R. H. W., Reeves, G. D., & Obara, T. (2002). Relativistic electron dynamics in the inner magnetosphere—A review. *Journal of Atmospheric and Terrestrial Physics*, *64*, 265–282.

Gjerloev, J. W. (2015). A global ground-based magnetometer initiative. *Eos*, *90*, 230–231. https://doi.org/10. 1029/2009EO270002

Gjerloev, J. W., Hoffman, R. A., Friel, M. M., Frank, L. A., & Sigwarth, J. (2004). Substorm behavior of the auroral electrojet indices. *Annales Geophysicae*, *22*, 2135–2149.

Kelbert, A., Balch, C. C., Pulkkinen, A., Egbert, G. D., Love, J. J., Rigler, E. J., & Fujii, I. (2017). Methodology for time-domain estimation of storm time geoelectric fields using the 3-D magnetotelluric response tensors. *Space Weather*, *15*, 874–894. https://doi.org/10.1002/2017SW001594

Kim, H.-J., & Chan, A. A. (1997). Fully adiabatic changes in storm time relativistic electron fluxes. *Journal of Geophysical Research*, *102*(A10), 22,107–22,116.

Liu, J., Angelopoulos, V., Zhang, X.-J., Turner, D. L., Gabrielse, C., Runov, A., et al. (2016). Dipolarizing flux bundles in the cis-geosynchronous magnetosphere: Relationship between electric fields and energetic particle injections. *Journal of Geophysical Research: Space Physics*, *121*, 1362–1376. https://doi.org/10.1002/2015JA021691

Love, J. J. (2012). Credible occurrence probabilities for extreme geophysical events: Earthquakes, volcanic eruptions, magnetic storms. *Geophysical Research Letters*, *39*, L10301. https://doi.org/10.1130/G32655.1

Lyons, L. R., Zesta, E., Xu, Y., Sánchez, E. R., Samson, J. C., Reeves, G. D., et al. (2002). Auroral poleward boundary intensifications and tail bursty flows: A manifestation of a large-scale ULF oscillation? *Journal of Geophysical Research*, *107*(A11), 1352. https://doi.org/10.1029/2001JA000242

Marin, J., Pilipenko, V., Kozyreva, O., Stepanova, M., Engebretson, M., Vega, P., & Zesta, E. (2014). Global Pc5 pulsations during strong magnetic storms: Excitation mechanisms and equatorward expansion. *Annales Geophysicae*, *32*, 319–3312. https://doi.org/10.5194/angeo-32-319-2014

McKay, A. J. (2003). Geoelectric fields and geomagnetically induced currents in the United Kingdom (PhD thesis), University of Edinburgh, UK.

McPherron, R. L., & Chu, X. (2016). Relation of the auroral substorm to the substorm current wedge. *Geosciences Letters*, *3*, 12.

McPherron, R. L., Russell, C. T., & Aubry, M. P. (1973). Satellite studies of magnetospheric substorms on August 15, 1968: 9. Phenomenological model for substorm. *Journal of Geophysical Research*, *78*(16), 3131–3149.

Mende, S. B., Harris, S., Frey, H., Angelopoulos, V., Russell, C., Donovan, E., et al. (2008). The themis array of ground-based observatories for the study of auroral substorms. *Space Science Reviews*, *141*, 357–387. https://doi.org/10.1007/s11214-008-9380-x

Murphy, K. R., Mann, I. R., Rae, I. J., Waters, C. L., Frey, H. U., Kale, A., et al. (2013). The detailed spatial structure of field-aligned currents comprising the substorm current wedge. *Journal of Geophysical Research: Space Physics*, *118*, 7714–7727. https://doi.org/10.1002/2013JA018979

Ngwira, C. M., Pulkkinen, A., Bernabeu, E., Eichner, J., Viljanen, A., & Crowley, G. (2015). Characteristics of extreme geoelectric fields and their possible causes: Localized peak enhancements. *Geophysical Research Letters*, *42*, 6916–6921. https://doi.org/10.1002/2015GL065061

Ngwira, C. M., Pulkkinen, A., Kuznetsova, M. M., & Glocer, A. (2014). Modeling extreme "Carrington-type" space weather events using three-dimensional MHD code simulations. *Journal of Geophysical Research: Space Physics*, *119*, 4456–4474. https://doi.org/10.1002/2013JA019661

Nishimura, Y., Lyons, L., Zou, S., Angelopoulos, V., & Mende, S. (2010). Substorm triggering by new plasma intrusion: THEMIS all-sky imager observations. *Journal of Geophysical Research*, *115*, A07222. https://doi.org/10.1029/2009JA015166

Onsager, T. G., Chan, A. A., Fei, Y., Elkington, S. R., Green, J. C., & Singer, H. J. (2004). The radial gradient of relativistic electrons at geosynchronous orbit. *Journal of Geophysical Research*, *109*, A05221. https://doi.org/10.1029/2003JA010368

Pirjola, R. (2002). Review on the calculation of the surface electric and magnetic fields and geomagnetically induced currents in ground based technological systems. *Surveys in Geophysics*, *23*, 71–90.

Pulkkinen, A., Bernabeu, E., Eichner, J., Viljanen, A., & Ngwira, C. M. (2015). Regional-scale high-latitude extreme geoelectric fields pertaining to geomagnetically induced currents. *Earth, Planets and Space*, *67*, 93. https://doi.org/10.1186/s40623-015-0255-6

Pulkkinen, A., & Kataoka, R. (2006). S-transform view of geomagnetically induced currents during geomagnetic superstorms. *Geophysical Research Letters*, *33*, L12108. https://doi.org/10.1029/2006GL025822

Pulkkinen, A., Lindahl, S., Viljanen, A., & Pirjola, R. (2005). Geomagnetic storm of 29–31 October: Geomagnetically induced currents and their relation to problems in the Swedish high-voltage power transmission system. *Space Weather*, *3*, S08C03. https://doi.org/10.1029/2004SW000123

Pulkkinen, A., Thomson, A., Clarke, E., & McKay, A. (2003). April 2000 geomagnetic storm: Ionospheric drivers of large geomagnetically induced currents. *Annales Geophysicae*, *21*, 709–717.

Rae, I. J., Mann, I. R., Murphy, K. R., Ozeke, L. G., Milling, D. K., Chan, A. A., et al. (2012). Ground-based magnetometer determination of in situ Pc4–5 ULF electric field wave spectra as a function of solar wind speed. *Journal of Geophysical Research*, *117*, A04221. https://doi.org/10.1029/2011JA017335

Reeves, G., Belian, R., Cayton, T., Henderson, M., Christensen, R., McLachlan, P., & Ingraham, J. (1997). Using Los Alamos geosynchronus energetic particle data in support of other missions. In G. Reeves, et al. (Eds.), *Satellite–ground based coordination source book* (pp. 263–272). Noordwijk, Netherlands: European Space Agency.

Reeves, G. D., & Henderson, M. (2001). The storm-substorm relationship: Ion injections in geosynchronous measurements and composite energetic neutral atom images. *Journal of Geophysical Research*, *106*(A4), 5833–5844.

Reeves, G. D., McAdams, K. L., Friedel, R. H. W., & O'Brien, T. P. (2003). Acceleration and loss of relativistic electrons during geomagnetic storms. *Geophysical Research Letters*, *30*(10), 1529. https://doi.org/10.1029/2002GL016513

Russell, C., Chi, P. J., Dearborn, D. J., Ge, Y. S., Kuo-Tiong, B., Means, J. D., et al. (2008). THEMIS ground-based magnetometers. *Space Science Reviews*, *141*, 389–412. https://doi.org/10.1007/s11214-008-9337-0

Sibeck, D. G., & Angelopoulos, V. (2008). THEMIS science objectives and mission phase. *Space Science Reviews*, *141*, 35–59. https://doi.org/10.1007/s11214-008-9393-5

Tsurutani, B. T., Hajra, R., Echer, E., & Gjerloev, J. W. (2015). Extremely intense (SML $\leq$ -2500 nT) substorms: Isolated events that are externally triggered? *Annales Geophysicae*, *33*, 519–524. https://doi.org/10.5194/angeocom-33-519-2015

Viljanen, A., Tanskanen, E. I., & Pulkkinen, A. (2006). Relation between substorm characteristics and rapid temporal variations of the ground magnetic field. *Annales of Geophysicae*, *24*, 725–733.

Weygand, J. M., Amm, O., Viljanen, A., Angelopoulos, V., Murr, D., Engebretson, M. J., et al. (2011). Application and validation of the spherical elementary currents systems technique for deriving ionospheric equivalent currents with the North American and Greenland ground magnetometer arrays. *Journal of Geophysical Research*, *116*, A03305. https://doi.org/10.1029/2010JA016177

Wolf, R. A. (1975). Ionosphere-magnetosphere coupling. *Space Science Reviews*, *17*, 537–562.

Wygant, J. R., Keiling, A., Cattell, C. A., Johnson, l. M., Lysak, R. L., Temerin, M., et al. (2000). Polar spacecraft based comparisons of intense electric fields and Poynting flux near and within the plasma sheet-tail lobe boundary to UVI images: An energy source for the aurora. *Journal of Geophysical Research*, *105*(A8), 18,675–18,692.

Yao, Z. H., Pu, Z. Y., Fu, S. Y., Angelopoulos, V., Kubyshkina, M., Xing, X., et al. (2012). Mechanism of substorm current wedge formation: THEMIS observations. *Geophysical Research Letters*, *39*, L13102. https://doi.org/10.1029/2012GL052055